Available online at www.sciencedirect.com
ScienceDirect
Journal of Volcanology and Geothermal Research 161 (2007) 352–361
Journal of volcanology and geothermal research
www.elsevier.com/locate/jvolgeores

Short Communication

Characterization of pyroclastic fall and flow deposits from the 1815 eruption of Tambora volcano, Indonesia using ground-penetrating radar

Lewis J. Abrams [a,*], Haraldur Sigurdsson [b]

[a] University of North Carolina, Center for Marine Science, 5600 Marvin Moss Lane, Wilmington, NC 28409, United States
[b] University of Rhode Island, Graduate School of Oceanography, Narragansett, RI 02882, United States

Received 3 August 2006; received in revised form 16 November 2006; accepted 24 November 2006
Available online 20 February 2007

Abstract

Ground-penetrating radar (GPR) is used to image and characterize fall and pyroclastic flow deposits from the 1815 eruption of Tambora volcano in Indonesia. Analysis of GPR common-mid-point (CMP) data indicate that the velocity of radar in the sub-surface is 0.1 m/ns, and this is used to establish a preliminary traveltime to-depth conversion for common-offset reflection profiles. Common-offset radar profiles were collected along the edge of an erosional gully that exposed approximately 1–2 m of volcanic stratigraphy. Additional trenching at select locations in the gully exposed the contact between the pre-1815 eruption surface and overlying pyroclastic deposit from the 1815 eruption. The deepest continuous, prominent reflection is shown to correspond to the interface between pre-eruption clay-rich soil and pyroclastics that reach a maximum thickness of 4 m along our profiles. This soil surface is distinctly terraced and is interpreted as the ground surface augmented for agriculture and buildings by people from the kingdom of Tambora. The correlation of volcanic stratigraphy and radar data at this location indicates that reflections are produced by the soil-pyroclastic deposit interface and the interface between pyroclastic flows (including pyroclastic surge) and the pumice-rich fall deposits. In the thickest deposits an additional reflection marks the interface between two pyroclastic flow units.

Keywords: ground-penetrating radar; Tambora volcano; Indonesia; pyroclastic flow

1. Introduction

The 1815 eruption of Tambora volcano in Indonesia is the largest historic explosive eruption, resulting in the loss of over 117,000 lives (de Jong Boers, 1996). This paper presents ground-penetrating radar (GPR) data collected near the Tambora Coffee Estate, Sumbawa, Indonesia at approximately 640 m elevation on the NW flank of Tambora volcano (Fig. 1). The primary objective of this survey was a feasibility study to use GPR to establish thickness variations in the pyroclastic deposit (e.g., Russell and Stasiuk, 2000) known to have buried the Kingdom of Tambora during the eruption of 1815 with the ultimate goal of providing sub-surface imagery of the site prior to archaeological excavations.

GPR is a relatively inexpensive, portable, non-invasive shallow sub-surface imaging tool. It has been applied to a wide variety of geological and engineering applications including imaging of the bedrock contact below glaciers (Clarke and Ross, 1989), environmental geophysics (Rea et al., 1994), and stratigraphy of

* Corresponding author.
E-mail address: abramsl@uncw.edu (L.J. Abrams).

0377-0273/$ - see front matter © 2006 Elsevier B.V. All rights reserved.
doi:10.1016/j.jvolgeores.2006.11.008

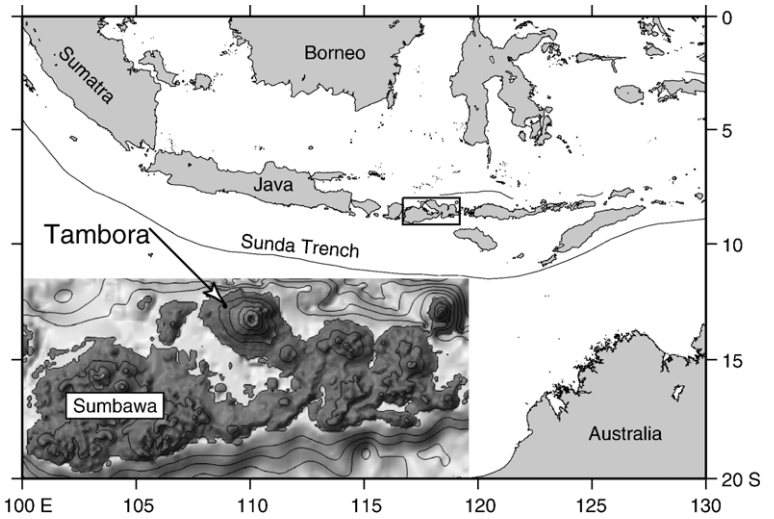

Fig. 1. Map of portions of the Indonesian archipelago and Australia. Box encloses the island of Sumbawa. Inset shows topography of Sumbawa with 500-m contours. Arrow locates survey location on the northwest flank of Tambora volcano. (GMT map, Wessel and Smith, 1995, Land elevation from the etopo30 digital elevation model, predicted bathymetry from Smith and Sandwell, 1997).

sediments and rock (Pratt and Miall, 1993; Jol and Meyers, 1996), GPR has also proven useful for investigating volcanic deposits (Russell and Stasiuk, 1997; Gómez-Ortiz et al., 2006). Another important application is in the field of archeology where GPR has been able to identify a variety of buried structures and provides a means for pre-excavation site characterization (Conyers and Goodman, 1997) including determination of the thickness of pyroclastic material overlying a pre-eruptive living surface (e.g., Russell and Stasiuk, 2000).

2. Data

2.1. Volcanic stratigraphy of the 1815 eruption exposed in Museum Gully

The largest volcanic eruption in recorded history resulted in a discharge of over 50 km^3 of trachyandesite magma during a 3-day period in April 1815. Detailed studies of the erupted products of this event on the island of Sumbawa in eastern Indonesia have been reported in Sigurdsson and Carey (1989), Sigurdsson and Carey (1992), Carey and Sigurdsson (1992). The varying eruption styles resulted in a sequence of volcanic ash and pumice falls, overlying a clay-rich pre-eruption soil, followed by multiple pyroclastic surge and pyroclastic flow deposits. Coastal exposures on the Sanggar peninsula reveal flow deposits of more than 20 m thickness. The volcanic stratigraphy at our study area is summarized in Fig. 2, following the nomenclature of Sigurdsson and Carey (1989).

2.2. GPR data acquisition and survey conditions

All GPR data were acquired using a Sensors and Software PulseEkko 100 with 1000 v transmitter. Common-offset profiles (COP) and common-midpoint profiles (CMP) were obtained using both 100 and 200 MHz antennae. Table 1 summarizes all vital acquisition parameters and profile locations are shown in Fig. 3.

Survey profiles are located on an unimproved logging road and within an adjacent eroded gully ("Museum Gully") approximately 1.5 km outside the Tambora Coffee Estate. The road surface and gully are the only areas clear of heavy underbrush and forest. The road surface lies directly on the 1815 pyroclastic deposit remaining after some minor erosion or removal during road construction. All data were collected during late July and early August during the dry season and no rain fell for the entire 5-week period when we were on site. CMP data were collected immediately after collection of associated COPs. The first COP and CMP data were collected using 100 MHz antennae. Real-time velocity analysis indicated that the pyroclastic deposits were relatively thin (2–4 m) here and so all subsequent lines were run using the higher resolution 200 MHz antennae. A total of 560 m of common-offset data and four CMP profiles encompassing 52 m were collected during 3 days devoted to GPR surveying.

Relative elevation profiles were obtained with eye-level and a stadia rod and were used to correct data for changing topography. Profile locations were established

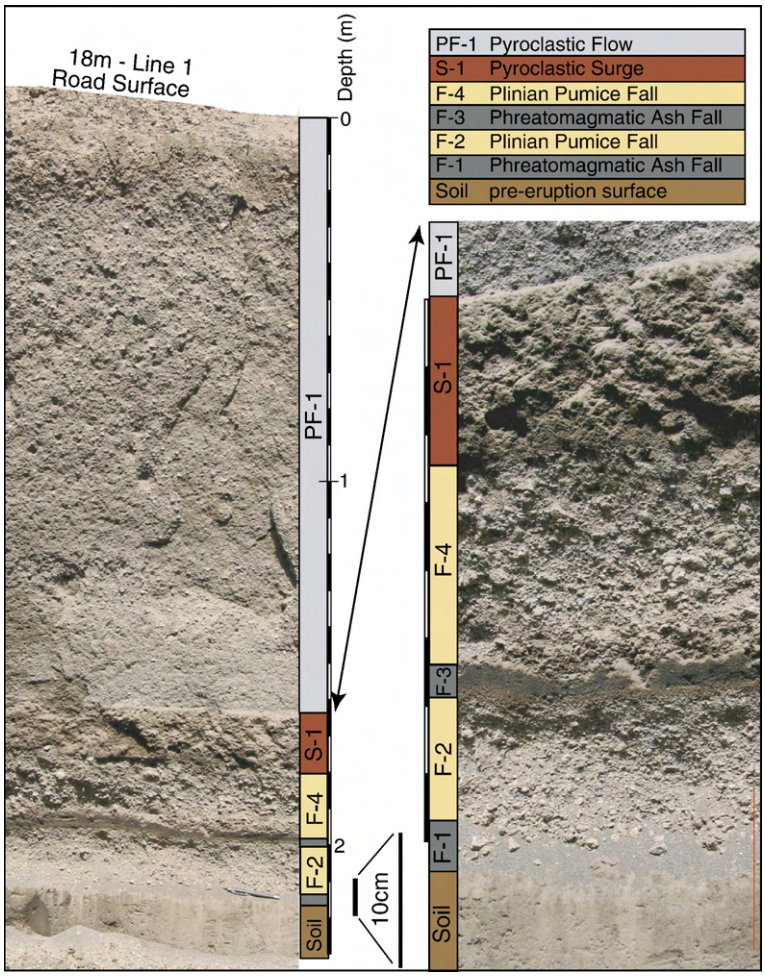

Fig. 2. Photograph of the gully wall and trench at 18–20 m along COP line 1 (Fig. 3) with correlation of volcanic units after Sigurdsson and Carey (1989).

with tape measure and compass relative to a central marker located with GPS (Fig. 3).

All radar data displayed have been corrected for signal saturation using a "Dewow" filter; this and other processing and display parameters are listed in Table 2. Static shifts have been applied to set traveltime equal to zero at the onset of the first positive deflection of the direct-air wave.

3. Results and discussions

3.1. Common mid-point (CMP) analysis

Radar data is analogous to seismic reflection data in that traveltime and amplitude of reflected signals are recorded. In order to convert traveltime to thickness or sub-surface depth, the velocity of radar in the deposit must be determined. We have estimated the average velocity of radar in the pyroclastic deposits by two different methods; CMP analysis and direct comparison of radar and lithostratigraphy at well-exposed sections.

Table 1
GPR acquisition parameters for PulseEkko 1000 v

Profile type and line #	Frequency (MHz)	Antennae separation (m)	Step size (m)	Traces averaged	Total length or separation (m)
COP 1	200	0.5	0.1	32	69.0
COP 1	100	1.0	0.25	32	67.75
COP 2	200	0.5	0.1	32	139.0
CMP 1	200	0.5	0.2	64	17.1
CMP 1	100	1.0	0.4	64	20.0
CMP 2	200	0.5	0.2	64	10.4
CMP 3	200	0.5	0.2	64	4.1

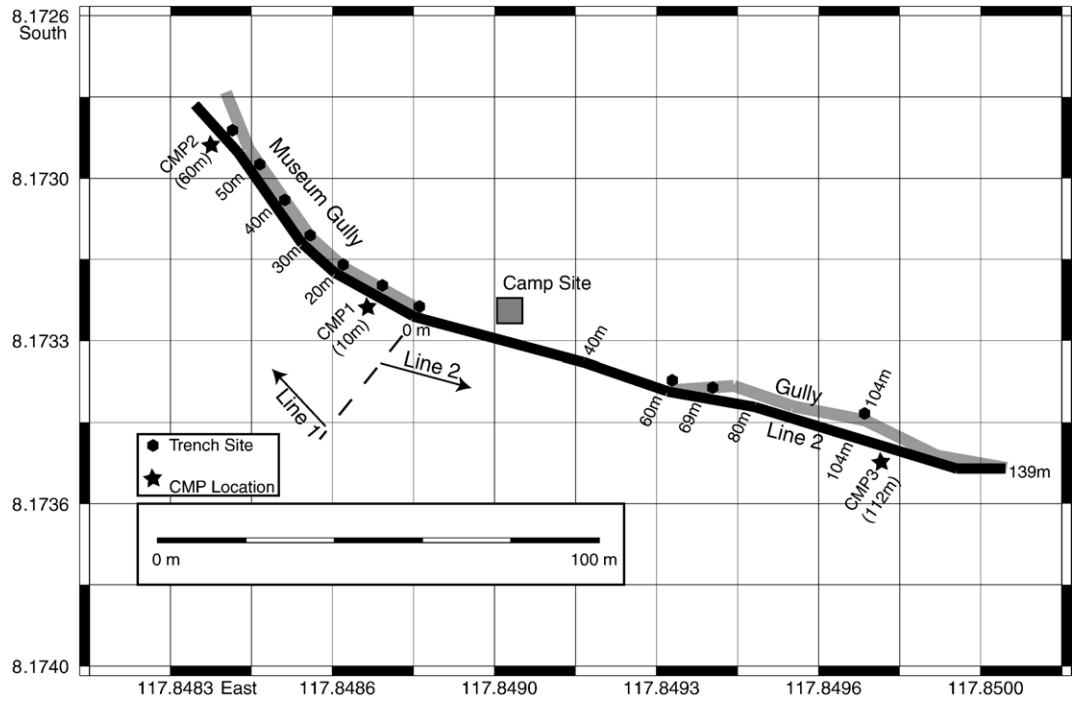

Fig. 3. Bold black line indicates 2-m wide road along which GPR survey lines 1 (0–69 m) and 2 (0–139 m) were obtained. Wide grey lines denote erosional gullies adjacent to road. Octagons indicate trench positions with distance along line in meters. CMP locations are labeled with stars.

In CMP surveys, the receiving and transmitting antennae are moved in opposite directions so as to increase the separation distance between each measurement, while maintaining a stationary mid-point. The geometry of CMP data acquisition allows collection of traveltime and travel distance data that are used to calculate velocity of both direct and reflected radar energy. On a standard plot of traveltime versus separation distance, direct air and ground waves will plot as straight lines, while reflected energy will plot as hyperbolae (Fig. 4). Thus, CMP data also serve as an important way to discriminate between energy reflected from surface objects (hyperbolic arrivals with $V = 0.3$ m/ns) from energy reflected from the sub-surface (hyperbolic arrivals with $V \ll 0.3$ m/ns).

Velocity of radar in resistive (low-loss) material is controlled by dielectric properties of the entire sub-surface that are generally not known. In fact, the dielectric properties (and therefore velocity) of earth material can change dramatically due to changes in porosity and porosity filling material (e.g., water versus air). Porosity conditions can change spatially and water content can also change temporally, thus it is important to obtain CMP data at various locations along a common-offset reflection profile and as close as possible in time so that both types of data are collected under the same saturation conditions.

An example of CMP data are displayed in Fig. 4 and the location of CMP profiles are shown in Fig. 3. Direct air and ground waves as well as reflected arrivals are visible on all CMPs. Fig. 4 also shows the correlation between CMP1 and COP data at 10 m range. Velocity analysis indicates the average velocity above the highest amplitude deep reflection is 0.105 m/ns. Velocity for the pyroclastic deposits from all CMPs ranges from 0.091 to 0.105 m/ns (Table 3). Interval velocities were not calculated.

Table 2
GPR display parameters

A permanent signal saturation correction (dewow) was applied to all data

Figure	Profile type and line#	Gain	Trace mix	Topographic correction depth scale
4	CMP Line 1	AGC [a]	10	N/A
5	COP Line 1	Autogain [b]	10	0.1 m/ns
7	COP Line 1	3dB [c]	3	0.1 m/ns
8	COP Line 2	3dB [c]	3	0.1 m/ns
9	COP Line 1	3dB [c]	3	0.1 m/ns

[a] Automatic Gain Control 100 ns window.
[b] Autogain scheme PulseEkko software.
[c] True relative amplitude preserved.

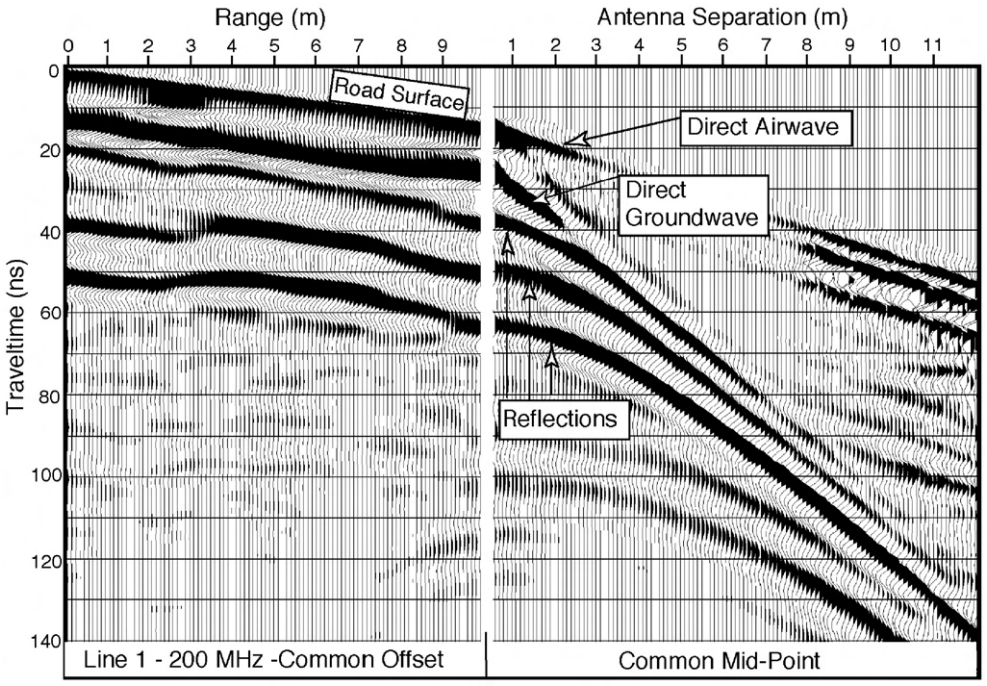

Fig. 4. Correlation between COP and CMP1 data obtained at 10 m range along line 1. Velocity analysis indicates an average velocity of 0.105 m/ns for pyroclastic material. Acquisition and display parameters are given in Tables 1 and 2.

3.2. Velocity estimates from direct comparison of radar and lithostratigraphy at well-exposed sections

CMP1 was acquired at 10 m along COP line 1. Applying a velocity of 0.105 m/ns results in a depth of 1.96 m and 2.60 m to the two deepest, high-amplitude, continuous reflections at 36 and 48 ns two-way travel time (nstwt) on COP data. The gully floor adjacent to these CMPs was ~1.9 m below the road surface, thus we expected to see a significant change in lithology, porosity and/or water content (i.e., contrasting electromagnetic properties) just below the gully surface. Trenching at 10 m along line 1 revealed a sharp contact between pyroclastic surge (S1) and the pumice fall deposits (F1 through F4 of Sigurdsson and Carey, 1989) at 1.82 m and between the pumice fall deposit overlying a moist, clay-rich layer (pre-1815 soil) at 2.26 m below the road surface, just 36 cm below the gully floor (Fig. 5). The overlap of predicted (1.96–2.6 m) and observed depth (1.82–2.26 m) led us to speculate that the arrivals at 36 and 48 nstwt are produced by electromagnetic contrasts across these interfaces. Assuming that the reflection at 36 nstwt corresponds to the outcrop depth of the surge/fall boundary at 1.82 m results in an average velocity above that interface of 0.099 m/ns, which is similar to, the velocity derived from CMP velocity analysis (0.105 m/ns). Table 3 lists average velocities of pyroclastic material from CMP data and from comparison of COP traveltime to measured thickness at trench sites. The primary result of such a comparison is that average velocities from

Table 3
Velocity estimates for pyroclastic flows

Line	Distance (m)	Observed PFD[a] thickness (m)	Velocity[b] of PFD (m/ns)	Velocity[c] of PFD (m/ns)
Line 2-CMP3	112	N/R	N/R	0.091
Line 2	104	3.1	0.099	
Line 2	70	1.5	0.109	
Line 2	59	0.46	0.108	
Line 1	0	1.9	0.097	
Line 1-CMP1	10	1.82	0.098	0.105
Line 1	20	1.71	0.087	
Line 1	30	1.86	0.088	
Line 1	40	1.31	0.090	
Line 1	50	1.17	0.110	
Line 1-CMP1	60	0.97	0.088	0.095
Average Velocity			0.097	0.100

[a] PFD-pyroclastic flow deposit including base surge.
[b] Velocity estimate from direct comparison of radar and lithostratigraphy at trench sites.
[c] Velocity from semblance analysis of CMP data.

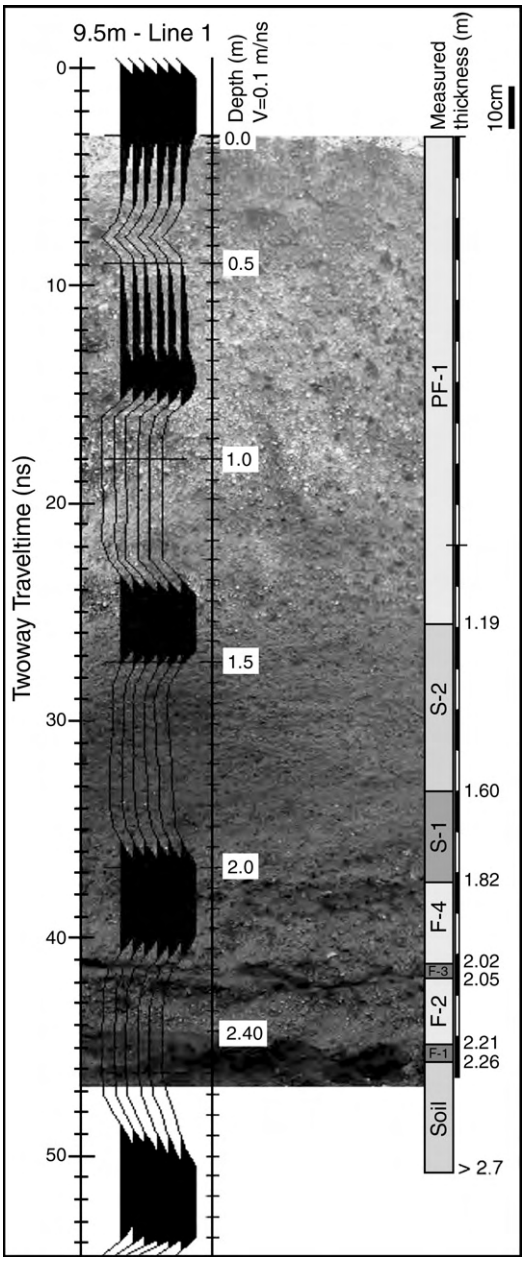

Fig. 5. Photograph of the gully wall and trench at 8–10 m along COP line 1 (Fig. 3) with correlation of volcanic units as shown in Fig. 2. Six traces of 200 MHz radargram displayed as wiggle trace and colored amplitude are superimposed. The non-linear depth scale for GPR results from the non-zero offset between transmitter and receiving antenna and is based on an average velocity of 0.1 m/ns. Acquisition and display parameters are given in Tables 1 and 2.

CMP data do not vary significantly along profile and that the observed variation in traveltime to these deepest reflections always correctly predicts the trend in observed thickness of the pyroclastic flow/surge and comes within 10–20 cm of values observed at trench sites in the gully. In addition, our estimated velocity values are similar to those reported in other locations for pyroclastic flow and surge deposits respectively of 0.1 m/ns (Russell and Stasiuk, 1997) and 0.095–0.1 m/ns (Cagnoli and Russell, 2000).

The ability of GPR to resolve the top and bottom of layers with contrasting electromagnetic properties include consideration of frequency and pulse length. The GPR signal is 1.5 cycles of the dominant frequency and thus the pulse length of the 200 MHz signal is ~7.5 ns. The earth, however, acts as a low pass filter and results from spectral analysis indicate that the reflected energy from our survey is approximately half the frequency of the outgoing pulse (i.e., reflections from the 200 MHz antennae have peak power at ~120 MHz, pulse length 12 ns) (Fig. 6). The low pass earth filter and the pulse length of ~12 ns effectively reduces the vertical resolution to ~1 m (at V=.1 m/ns). Electromagnetic impedance contrasts spaced closer than ~1 m will result in an interference pattern. Thus, we can place constraints on the variation in total thickness of pyroclastic material but not on variations within relatively thin (<0.5 m) individual pumice and ash fall units (F1 through F4). Detailed correlation of this nature will require higher frequency antennae and synthetic radargrams.

Closer inspection of the CMP, COP and lithostratigraphy data at the 10 m trench site (Fig. 5) indicates that the contact between the flow/surge and fall deposits represents a contrast in electromagnetic properties that results in the continuous, positive amplitude reflection at ~36 nstwt and that the fall/soil interface must lie within the following trough (negative amplitude). This is consistent with a phase reversal reflection produced by the expected decrease in velocity resulting from an increase in water content in the moist, clay-rich soil. Any such correlation highlights the potential pitfalls inherent when matching radar and lithostratigraphy without a synthetic seismogram based on actual electromagnetic values.

In summary, time section COPs accurately portray relative thickness variations of pyroclastic material over clay-rich soil, however the use of any single average velocity will not allow centimeter-scale depth matching to lithostratigraphy measured at specific locations. Depths reported in following section are calculated using an average velocity of 0.1 m/ns, because only slight lateral variations in average velocity are recognized (Table 3).

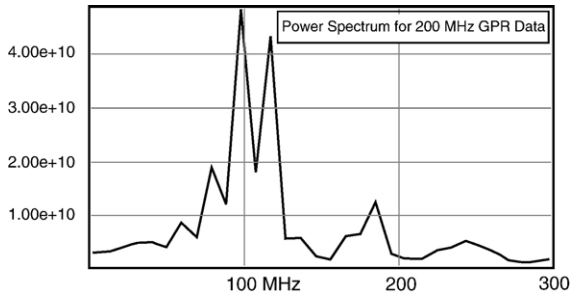

Fig. 6. Power spectrum of a 10-trace mix (0–80 ns window) from 200 MHz COP line 2. Peak power is observed at 120 MHz.

3.3. Radar and volcanic stratigraphy

Common-offset profile data are presented in two line segments relative to the 0 m GPS station (Fig. 3). Line 1 (100 MHz and 200 MHz) is a 69 m-long survey running Northwest along the road bed parallel to Museum Gully, line 2 (200 MHz) is a 140 m-long segment running Southeast along the road surface, also paralleling a gully (Figs. 7 and 8).

Fig. 4 shows the correlation between CMP and COP data. The first two high-amplitude continuous arrivals on COP data correspond to linear arrivals in CMP data indicating that this energy is from direct air and ground waves respectively. Energy arriving at greater travel-times in COP data corresponds to hyperbolic arrivals in CMP data, indicating that these are reflected energy from sub-surface contrasts in electromagnetic properties (i.e. $V = 0.1$ m/ns < 0.3 m/ns).

Common-offset profiles displayed at true relative amplitude or with automatic gain control (AGC) show a continuous high-amplitude interference pattern consisting of positive/negative/positive varying from 20–80 nstwt below ground level (Figs. 7 and 8). Correlations between radar and volcanic stratigraphy (Fig. 5) indicate that the first positive deflection (36 nstwt) corresponds to the interface between flow and fall and that the fall/soil interface is marked by the central trough (44 nstwt). Very little energy is returned from deeper in the section even using 100 MHz antennae (Fig. 9), which is consistent with the expected attenuation of radar signal in a moist clay-rich soil. The pyroclastic

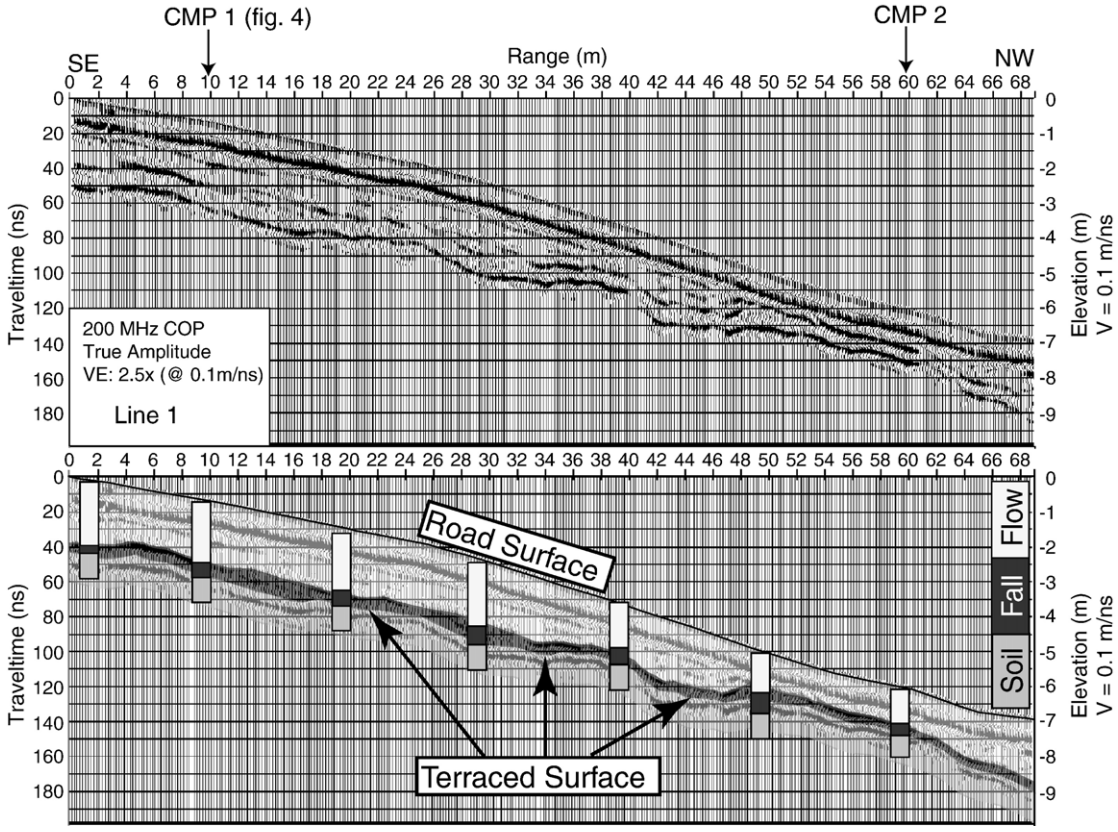

Fig. 7. Topographically corrected COP data from line 1. Volcanic units observed on the gully wall and in trench sites are superimposed. Flow designation includes basal surge (Fig. 2). Acquisition and display parameters are given in Tables 1 and 2.

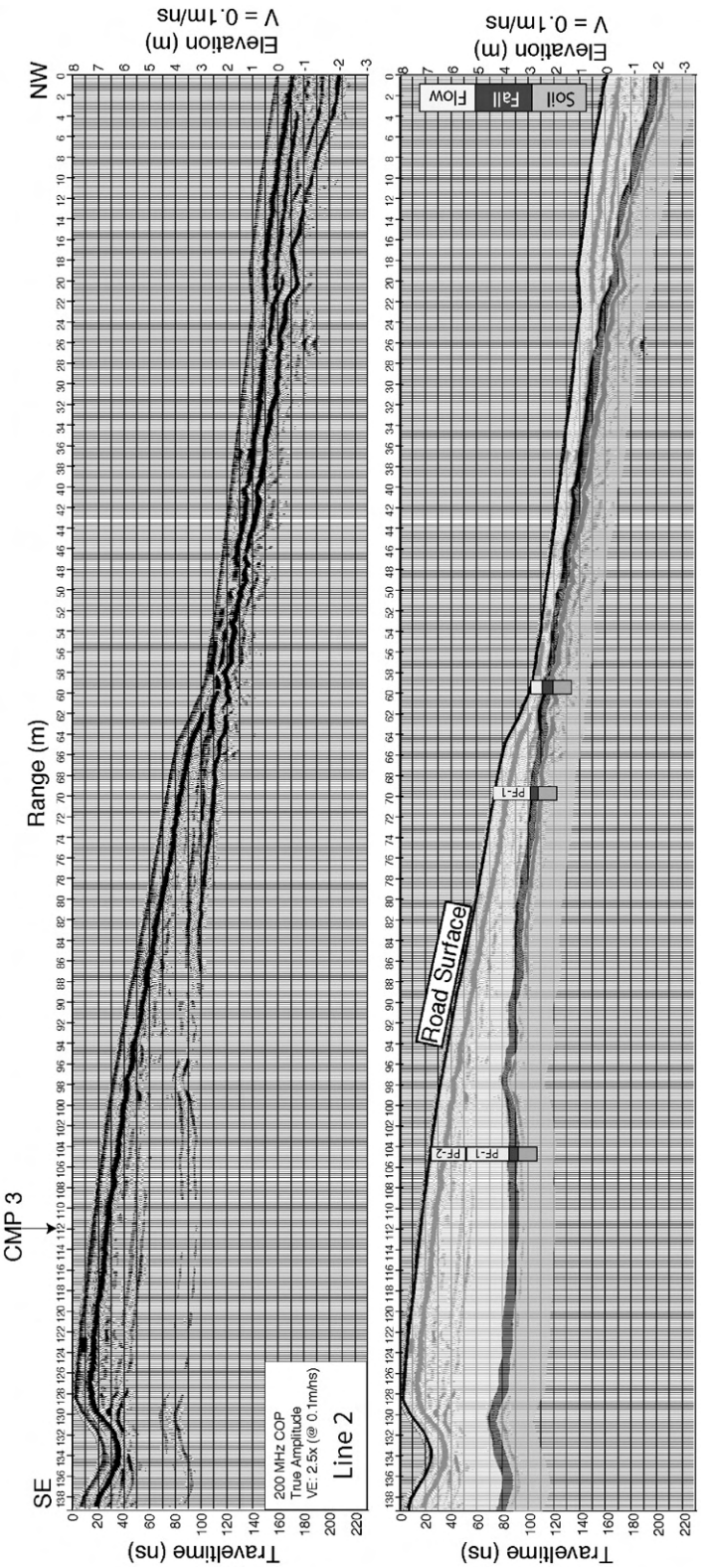

Fig. 8. Topographically corrected COP data from line 2. Volcanic units observed on the gully wall and in trench sites are superimposed. Acquisition and display parameters are given in Tables 1 and 2.

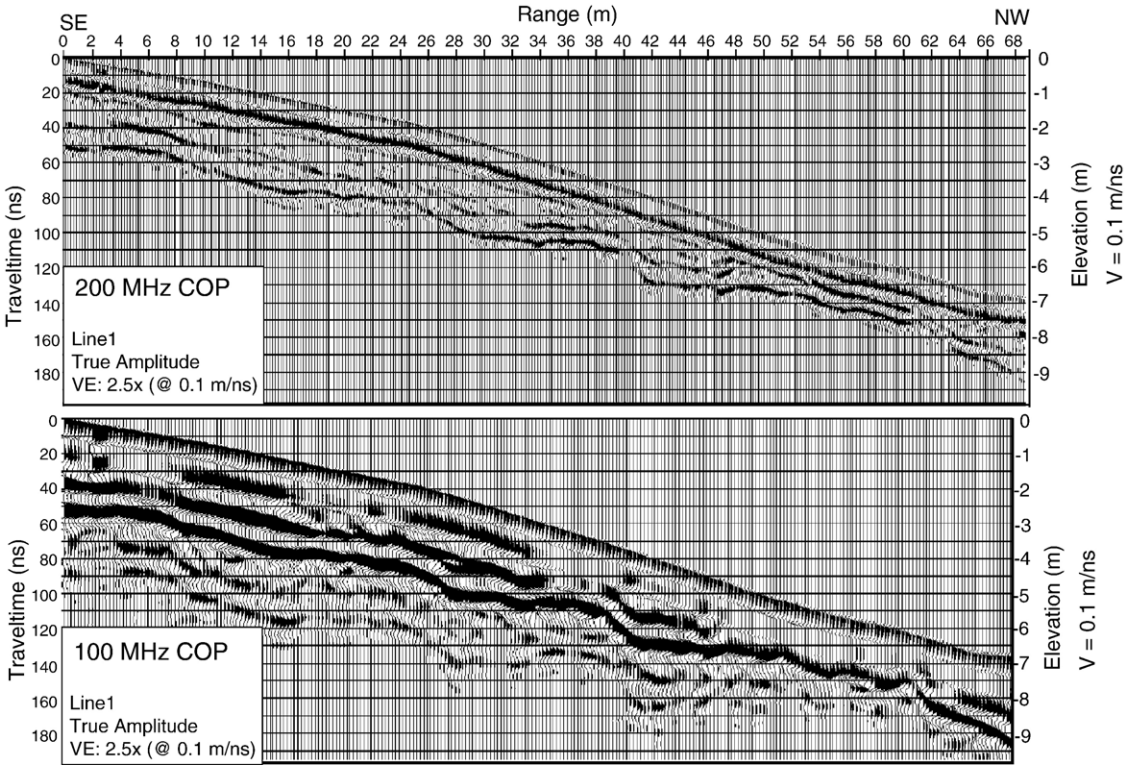

Fig. 9. Comparison of topographically corrected COP data from line 1 using 200 MHz antennae (top) and 100 MHz antennae (bottom).

flow deposit (PF-1) is characterized by a relative transparent radar image, except along line 2 from 100 to 138 m range, where the pyroclastic flow unit noticeably thickens (Fig. 8). In this section a continuous high-amplitude reflection separates two relatively transparent intervals. At the 104 m trench site the depth of this reflection is ~1.46 m (at 0.1 m/ns) but no obvious lithologic or grain size change is apparent on the gully wall. We speculate that this reflection marks the contact between two different pyroclastic flow units that combine to create the 3.1 m thick pyroclastic flow observed at the trench site at 104 m (Fig. 8). Pumice clasts of <7 cm are observed in the pyroclastic flow. This is much smaller than the scattering dimension for radar of this wavelength and is consistent with the transparent nature of the radar image. The upper pyroclastic flow unit (designated PF-2) appears to pinch out at ~100 m on line 2 and extends to the southeast beyond our survey area (Fig. 8). The lower PFD (PF-1) thins dramatically between 22–62 m along line 2 where the direct ground wave and the reflection from the pyroclastic flow/fall appear to merge. The thinning pyroclastic flow deposit is most likely a consequence of removal during road construction. The fall deposit however appears to maintain a relatively uniform thickness, draping over the pre-1815 eruption soil along all COPs. This indicates that in general the fall deposit was not extensively eroded by subsequent pyroclastic flows.

Common-offset profile line 1 (Fig. 7) continues 69 m to the Northwest along the road surface, adjacent to Museum Gully, where trenching was done every 10 m (Figs. 2 and 3). Trenching along this profile reveals that the pyroclastic flow unit includes a distinct pyroclastic surge deposit that varies in thickness from 0.0–0.65 m (e.g., S1, Fig. 2). The reflections associated with the fall/soil and surge/fall interfaces appear as a series of distinct slope changes or steps while the overlying pyroclastic flow deposits (PF-1, S1) appear to fill in over this pre-existing morphology (Fig. 7). The stepped structure is nearly identical on both migrated and un-migrated data and is interpreted as terraces constructed in the pre-eruption soil presumably providing level surfaces for irrigation, agriculture and housing. Terracing is not observed on COP 2 (Fig. 8).

Data from both 100 and 200 MHz antennae were collected along identical paths on line 1 (Fig. 9). The images of the fall/soil and surge/fall interfaces are similar except between 48 to 65 m range where the pyroclastic flow and fall deposits are thinnest. At this

location the deepest, high-amplitude, continuous event imaged on the 100 MHz profile is a negative/positive/negative arrival with the positive amplitude peak located just below the fall/soil interface. Apparently the 100 MHz data are imaging the negative impedance boundary created at the top of the soil but not resolving any contrasts in the pyroclastic section. The 100 MHz antennae do provide greater depth penetration revealing some discontinuous, low-amplitude arrivals extending to ~100 nstwt, much deeper in the section than sampled by trenching.

4. Conclusion

1) Velocity analysis of common-mid-point data indicate velocity in pyroclastic material from the 1815 eruption of Tambora ranges from 0.091–0.105 m/ns. These values are consistent with velocities derived from visual correlations between radar stratigraphy and volcanic stratigraphy at discrete trench sites.
2) Common-offset profiles reveal that the total thickness of pyroclastic material overlying the pre-eruption soil varies along profile from ~0.5 m to over 4 m. Thickness of the fall deposits are relatively uniform, appear to drape the underlying pre-eruption soil surface, and are not significantly eroded by the subsequent pyroclastic flow.
3) Distinct slope changes in reflections associated with the soil/fall interface are interpreted as terraces cut into the pre-eruption soil surface to accommodate agriculture and/or housing.
4) Constraints on thickness variations within relatively thin (<0.5 m) individual fall units (F1 through F4) will require higher frequency antennae and synthetic radargrams.

Acknowledgements

We are grateful to the people of Tambora village for their friendship and cooperation during our six-week expedition. We are especially thankful to Dr. Igan Sutawidjaja, Directorate of Volcanology and Geohazards Mitigation, Indonesia, who aided us in all aspects of the expedition. Intermap Inc. kindly provided airborne radar images and digital elevation models of Tambora volcano. The personnel at Sensors and Software Inc. provided valuable advise for maintenance and operation of GPR equipment. We also thank Dr. Kelly Russell and Dr. David Gómez-Ortiz for encouraging and helpful reviews.

References

Cagnoli, B., Russell, J.K., 2000. Imaging the sub-surface stratigraphy in the Ubehebe hydrovolcanic field (Death Valley, California) using ground-penetrating radar. J. Volcanol. Geotherm. Res. 96, 45–56.

Carey, S., Sigurdsson, H., 1992. Generation and dispersal of tephra from the 1815 eruption of Tambora volcano, Indonesia. The Sea off Mount Tambora. Mitt. Geol. Paleont. Inst. Univ. Hamburg Heft, vol. 70, pp. 207–226.

Clarke, K., Ross, G., 1989. Radar imaging of glaciovolcanic stratigraphy, Mount Wrangell caldera, Alaska: interpretation, model and results. J. Geophys. Res. 94, 7237–7249.

Conyers, L.B., Goodman, D., 1997. Ground-penetrating radar: an Introduction for Archaeologists. Altamira Press, London.

de Jong Boers, B., 1996. Mount Tambora in 1815: a volcanic eruption in Indonesia and its aftermath. Cornell Modern Indonesia Project, vol. 60, No. 2, pp. 36–60. Ithaca, N.Y.

Gómez-Ortiz, D., Martín-Velázquez, S., Martín-Crespo, T., Márquez, A., Lillo, J., López, I., Carreño, F., 2006. Characterization of volcanic materials using ground-penetrating radar: a case study at Teide volcano (Canary Islands, Spain). J. Appl. Geophys. 59 (1), 63–78.

Jol, H.M., Meyers, R.A., 1996. Digital Ground-penetrating radar (GPR): a new geophysical tool for coastal barrier research (examples from the Atlantic, Gulf, and Pacific coasts USA). J. Coast. Res. 12, 960–968.

Pratt, B., Miall, A., 1993. Anatomy of a bioclastic grainstone megashoal (Middle Silurian, southern Ontario) revealed by ground-penetrating radar. Geology 21, 223–226.

Rea, J., Knight, R., Ricketts, B., 1994. Ground-penetration radar survey of the Brookswood aquifer, Fraser Valley, British Columbia. Geol. Surv. Can. Pap. 1994-A, 211–216.

Russell, J., Stasiuk, M., 1997. Characterization of volcanic deposits with ground-penetrating radar. Bull. Volcanol. 58, 515–527.

Russell, J., Stasiuk, M., 2000. Ground-penetrating radar mapping of Minoan volcanic deposits and the Late Bronze Age paleotopography, Thera, Greece. In: McGuire, W., et al. (Eds.), The Archeology of Geological Catastrophes. Geol. Soc. Lond. Spec. Pub., vol. 171, pp. 105–121.

Sigurdsson, H., Carey, S., 1989. Plinian and co-ignimbrite tephra fall from the 1815 eruption of Tambora volcano. Bull. Volcanol. 51, 243–270.

Sigurdsson, H., Carey, S., 1992. Eruptive history of Tambora volcano, Indonesia. The Sea off Mount Tambora. Mitt. Geol. Paleont. Inst. Univ. Hamburg Heft, vol. 70, pp. 187–206.

Smith, W.H.F., Sandwell, D.T., 1997. Global seafloor topography from satellite altimetry and ship depth soundings. Science 277, 1956–1962.

Wessel, P., Smith, W.H.F., 1995. New version of the Generic Mapping Tools released. Eos Trans. AGU 76 (329).